Benchmarking D-Wave Quantum Annealers: spectral gap scaling of maximum cardinality matching problems

Cameron Robert McLeod[1] and Michele Sasdelli[1][0000−0003−1021−6369]

Australian Institute for Machine Learning, The University of Adelaide, Australia
cameron.mcleod@student.adelaide.edu.au
michele.sasdelli@adelaide.edu.au

Abstract. Quantum computing, in particular Quantum Annealing (QA), provides a theoretically promising alternative to classical methods for solving combinatorially difficult optimization problems. In particular, QA is suitable for problems that can be formulated as a Quadratic Unconstrained Binary Optimization (QUBO) problem, such as SAT, graph colouring and travelling salesman. With commercially available QA hardware, like that offered by D-Wave Systems (D-Wave), reaching scales capable of tackling real world problems, it is timely to assess and benchmark the performance of this current generation of hardware. This paper empirically investigates the performance of D-Wave's 2000Q (2048 qubits) and Advantage (5640 qubits) quantum annealers in solving a specific instance of the maximum cardinality matching problem, building on the results of a prior paper that investigated the performance of earlier QA hardware from D-Wave. We find that the Advantage quantum annealer is able to produce optimal solutions to larger problem instances than the 2000Q. We further consider the problem's structure and its implications for suitability to QA by utilising the Landau-Zener formula to explore the potential scaling of the diabatic transition probability. We propose a method to investigate the behaviour of minimum energy gaps for scalable problems deployed to quantum annealers. We find that the minimum energy gap for our target QA problem does not scale favourably. This behaviour raises questions as to the suitability of this problem for benchmarking QA hardware, as it potentially lacks the nuance required to identify meaningful performance improvements between generations.

Keywords: D-Wave · Quantum Annealing · Maximum Matching · Landau-Zener.

1 Introduction

The promise of quantum computing has been a tantalising prospect ever since the concept of utilising quantum behaviour to perform computation was first proposed, most notably in the early 1980s with the work of Paul Benioff [2, 4, 3] and Richard Feynman [10]. Since the inception of this idea there has been significant effort invested, and subsequent advances in hardware, however, it remains a speculative area with no clear indication if the promise of quantum computing will be realised [8] or if classical computing will reign supreme.

There are a number of competing approaches to quantum computing including Quantum Gate Array (QGA) [18], One-way Quantum Computers (OQC) [20], more

ICCS Camera Ready Version 2022
To cite this paper please use the final published version:
DOI: 10.1007/978-3-031-08760-8_13

exotic and theoretical Topological Quantum Computers (TQC) [14], Adiabatic Quantum Computers (AQC) [1] and Quantum Annealing (QA) approaches [9] and many others such as those covered in [19]. While the QGA model is arguably the most investigated, QA has shown recent promise with commercially available hardware reaching scales, i.e. number of qubits, with the potential of tackling useful real world problems [26, 13]. QA as described in [24], inhabits a regime that is intermediate between the idealised assumptions of universal AQC and unavoidable experimental compromises.

The contribution of this work is mainly twofold. We first extend the work of [23] to the latest QA hardware from D-Wave and contrast the performance between quantum annealers. We then consider the structure of the specific problem we have utilised to assess the quantum annealer performance. It is known that as the energy gap between two energy states of a quantum system decreases, the greater the likelihood the system will 'jump' from one to the other [28]. We utilise the Landau-Zener formula to calculate the expected diabatic transition probabilities for increasing problem sizes. We estimate the scaling of the problem's minimum energy gap, that is the minimum energy gap between the ground state and the first excited state, and discuss the implications for suitability to benchmark QA. We hope that this work forms a building block in the ongoing assessment and benchmarking of quantum annealer performance.

2 Quantum Annealing on D-Wave

The QA implementation used by D-Wave is of the form shown in Equation 1 where $\hat{\sigma}_x^{(i)}$ and $\hat{\sigma}_z^{(i)}$ are Pauli matrices operating on a qubit, q_i, and h_i and $J_{i,j}$ are the qubit biases and coupling strengths.

$$\mathcal{H}_{ising} = -\frac{A(s)}{2}\left(\sum_i \hat{\sigma}_x^{(i)}\right) + \frac{B(s)}{2}\left(\sum_i h_i \hat{\sigma}_z^{(i)} + \sum_{i>j} J_{i,j}\hat{\sigma}_z^{(i)}\hat{\sigma}_z^{(j)}\right) \tag{1}$$

Using D-Wave terminology [17] the initial Hamiltonian is called the tunnelling Hamiltonian and is in its lowest energy state when all qubits are in a superposition state of 0 and 1. The final Hamiltonian, also called the problem Hamiltonian, encodes the spin problem to be optimised, Equation 2, by extending it from discrete spins to quantum states. The ground state of the problem Hamiltonian corresponds to the solution of the Ising problem. Initially the quantum annealer starts in the lowest energy state of the tunnelling Hamiltonian and slowly introduces the problem Hamiltonian, i.e. the annealing cycle begins at $s = 0$ with $A(s) \gg B(s)$ and ends at $s = 1$ with $A(s) \ll B(s)$.

$$\mathrm{E}_{ising}(s) = \sum_i h_i s_i + \sum_{i>j} J_{i,j} s_i s_j \tag{2}$$

Once the annealing cycle is completed, $s = 1$, the $\hat{\sigma}_z^{(i)}$ can be replaced by classical spin variables, $s_i = \pm 1$. The energy of the system is then described as per Equation

ICCS Camera Ready Version 2022
To cite this paper please use the final published version:
DOI: 10.1007/978-3-031-08760-8_13

2 with the s_i's corresponding to the solution for the target problem. If the system has remained in the ground state then the corresponding values of the s_i's represent the optimal solution to the target problem.

2.1 QUBO formulation

QA requires that Hamiltonians be written as the quantum version of the Ising spin glass [21]. Ising spin glasses often go by the name of Quadratic Unconstrained Binary Optimisation (QUBO) problems [16, 12]. A general QUBO model is expressed as an optimisation problem, as shown in Equation 3, where x is a vector of binary decision variables and Q is a square matrix:

$$minimise/maximise\ y = x^T Q x. \tag{3}$$

Quadratic penalties are added to the objective function to impose constraints on the problem. These penalties are constructed such that their contribution is zero for feasible solutions and some positive amount for infeasible solutions.

Consider the maximum cardinality matching problem, whose goal is, for some graph, G, to find a matching containing as many edges as possible such that each vertex is adjacent to at most one of the selected edges. The maximum matching problem, for a graph, $G = (V, E)$, can be represented as shown in Equation 4.

$$\text{Maximise} \sum_{e \in E} x_e \quad s.t. \quad \forall v \in V, \sum_{e \in E(v)} x_e \leq 1 \tag{4}$$

where $x_e \in \{0, 1\}$ and $E(v)$ denotes the set of edges which have v as an endpoint.

Once the target problem has been formulated as a QUBO, it is then able to be implemented and run on a quantum annealer. To implement the QUBO on the quantum annealer it is first converted into an equivalent Ising problem, which requires the mapping of binary variables, $x_i \in \{0, 1\}$, to spin variables, $s_i \in \{-1, 1\}$ via the relation $s_i = 2x_i - 1$. These spin variables are then mapped to physical qubits on the QPU. Many of these implementation details are handled by the API associated with the quantum annealer as is the case with submitting problems to D-Wave's quantum annealers.

3 Maximum Cardinality Matching

The goal of the maximum matching problem is to find, for some graph, a matching containing as many edges as possible, that is, a maximum cardinality subset of the edges, such that each vertex is adjacent to at most one edge of the subset. More formally the problem can be stated as for some (undirected graph), $G = (V, E)$, the maximum matching problem asks for $M \subseteq E$ such that $\forall e, e' \in M^2, e \neq e'$ we have that $e \cap e' = \emptyset$ and such that $|M|$ is maximum [15].

3.1 Graph Family

ICCS Camera Ready Version 2022
To cite this paper please use the final published version:
DOI: 10.1007/978-3-031-08760-8_13

As per [23] a specific family of graphs are utilised for the application of the maximum matching problem. This graph family, G_n, consists of alternating layers of sparsely and densely connected nodes where the number of rows are equal to $(n+1)$ and the number of layers equal to $(2n+1)$. The total number of edges for a specific G_n graph is $(n+1)^3$ and the number of nodes is $2(n+1)^2$. As an example, the G_1 and G_2 graphs are shown in Figure 1. A rigorous definition of this graph family can be found in [22].

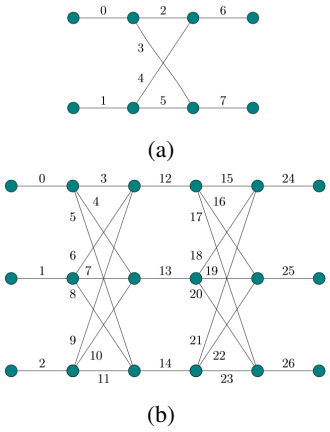

Fig. 1: Schemes representing the G_1(a) and G_2(b) graphs.

There are two main reasons for the selection of this family of graphs. Firstly, it is trivial to see that a maximum matching for G_n consists of all the edges in the sparsely connected layers. It is therefore easy to check solutions returned by a quantum annealer. Secondly, the work presented in [22] shows that the expected number of iterations required by a class of annealing algorithms to reach a maximum matching is in $O(\exp(n))$. It is these two properties that make this graph family an interesting testing ground for quantum annealers.

3.2 QUBO Formulation

To formulate the maximum matching problem as a QUBO we must incorporate the constraints of Equation 4 into the objective function. The optimisation problem is looking to incentivise the inclusion of all edges, this corresponds to the diagonal terms in Q. The constraint that selected edges are not adjacent to other selected edges corresponds to the off-diagonal terms in Q. An example QUBO formulation for a G_1 graph is shown in Equation 5, where we have chosen -1, being a minimisation problem, to represent the value of an included edge and a penalty term of P for adjacent edges. A vector of $[1, 1, 0, 0, 0, 0, 1, 1]$ minimises the value of Equation 5, pending a sufficiently large P. Given an arbitrary graph, the QUBO formulation to find a maximum matching would require that the ratio of off-diagonal to diagonal elements be greater than 1. Naturally the penalty of violating a constraint must outweigh the benefit of incorporating another edge into the solution. In our formulation we opt for a value of $P = 2$. This value was chosen to avoid excessive scaling of biases and coupling values, as at implementation time on the annealer D-Wave re-scales h_i and $J_{i,j}$ values between [-2,2] and [-1,1] respectively. The choice of P is itself an area that warrants further investigation and an optimal choice will likely depend on the specific problem structure.

We refer to the formulation shown in Equation 5 as the 'general' formulation and the formulation in [23] as the 'prior' formulation from here out. This distinction is due to [23] utilising $1 + 2|E|$ and $-2|E|$ for their diagonal and off-diagonal values, respectively, in Q. We note that the prior formulation is valid for the utilised G_n graphs but that it is not necessarily true for general graphs given $\frac{2|E|}{1+2|E|} < 1$. We provide

ICCS Camera Ready Version 2022
To cite this paper please use the final published version:
DOI: 10.1007/978-3-031-08760-8_13

performance comparisons for both QUBO formulations, to provide continuity in the performance benchmark dataset and also to investigate any impacts on solution quality when a general formulation is used.

$$\text{Min} y = \begin{bmatrix} x_0 \\ x_1 \\ x_2 \\ x_3 \\ x_4 \\ x_5 \\ x_6 \\ x_7 \end{bmatrix}^\top \begin{bmatrix} -1 & 0 & P & P & 0 & 0 & 0 & 0 \\ 0 & -1 & 0 & 0 & P & P & 0 & 0 \\ 0 & 0 & -1 & P & P & 0 & P & 0 \\ 0 & 0 & 0 & -1 & 0 & P & 0 & P \\ 0 & 0 & 0 & 0 & -1 & P & P & 0 \\ 0 & 0 & 0 & 0 & 0 & -1 & 0 & P \\ 0 & 0 & 0 & 0 & 0 & 0 & -1 & 0 \\ 0 & 0 & 0 & 0 & 0 & 0 & 0 & -1 \end{bmatrix} \begin{bmatrix} x_0 \\ x_1 \\ x_2 \\ x_3 \\ x_4 \\ x_5 \\ x_6 \\ x_7 \end{bmatrix} \tag{5}$$

4 Improved QPU Topology

One of the key changes in hardware from D-Wave has been the improvement in the physical QPU architecture (or topology). D-Wave refers to the two most recent architectures as Chimera (present in the 2000Q and older models) and Pegasus (present in the Advantage) [6]. The Chimera architecture consists of recurring $K_{4,4}$, bipartite graph unit cells which are coupled together and each qubit is physically coupled to 6 other qubits. The Pegasus architecture, present in the Advantage quantum annealer, increases the interconnection density with each qubit being connected to 15 other qubits. This increase in qubit connectivity has positive implications with respect to chain lengths and minor embedding.

When looking to solve an arbitrary problem on a D-Wave quantum annealer the problem's structure may not naturally match the annealer's topology, as such the problem needs to be 'embedded'. Physical qubits need to be linked, or coupled, to form 'chains' each representing a logical variable of original problem [5]. This introduces the issue of chain breaks in the solutions found by the quantum annealer. Resolving these chain breaks to find a consensus solution is typically achieved via empirical approaches, such as majority voting by the qubits in the broken chain.

5 Quantum Annealing Experiments

To conduct our experiments we made use of D-Wave's open-source SDK, Ocean, and the quantum annealers 'DW_2000Q_6', 'Advantage_system1.1' and 'Advantage_system4.1'. Where we refer to 'Advantage' it is a reference to both the 1.1 and 4.1 variants, where we refer to a specific annealer the version number is specified. For all experiments we utilised, unless specified otherwise, the default annealing duration of $20\mu s$ and 10,000 samples (annealing cycles). Similar to [23] we note that both shorter and longer annealing durations had negligible impacts, although a more nuanced analysis could be of future benefit. We also utilised the default chain strength, which is calculated using D-Wave's 'uniform torque compensation'.

ICCS Camera Ready Version 2022
To cite this paper please use the final published version:
DOI: 10.1007/978-3-031-08760-8_13

6 Results Overview

Experimental results on the newest Advantage architecture are shown in Table 1. Up to the G3 graph, the quantum annealer is able to obtain the optimal solution. It is not guaranteed that the solutions returned will be valid for the original problem i.e. they may violate the problem constraints. As noted in [23] a post processing step would be required when using QA to ensure results produce valid matchings. Checking the validity of solutions is trivial and it is an insightful metric to assess the performance of QA hardware. Table 2 provides a summary of the number of valid solutions returned out of the 10,000 annealing cycles. An insight of these results is that our general QUBO formulation produces significantly more valid solutions. We postulate that the quantity of valid solutions is directly correlated to the ratio between diagonal and off-diagonal terms in our Q matrix. We also note that both the 2000Q and Advantage quantum annealers produce valid results for the G_3 graph, whereas the 2X failed to produce a single valid matching, demonstrating an improvement in the hardware's capability, albeit minor.

Table 1: Results Advantage - General and Prior QUBO Formulations (All Samples)

	Best	Worst	Mean	Med.	St.Dev.	Best	Worst	Mean	Med.	St.Dev.
	2000Q (General)					2000Q (Prior)				
G1	-4	-1	-4.0	-4	0.2	-68	-36	-67.9	-68	1.1
G2	-9	-4	-7.9	-8	0.8	-495	-279	-451.5	-442	37.8
G3	-16	-5	-11.4	-12	1.3	-2064	-1046	-1563.2	-1553	108.0
G4	-21	-5	-16.1	-16	2.0	-5526	-3279	-4579.6	-4527	292.1
	Advantage1.1 (General)					Advantage1.1 (Prior)				
G1	-4	-2	-4.0	-4	0.2	-68	-52	-68.0	-68	0.6
G2	-9	-2	-7.1	-7	1.0	-495	-227	-428.0	-441	43.3
G3	-16	-3	-11.2	-11	1.6	-2064	-1042	-1592.8	-1554	127.5
G4	-22	-1	-13.9	-14	3.0	-5527	-2528	-4281.0	-4279	387.6
G5	-29	6	-13.6	-14	4.7	-12137	-4800	-9373.3	-9545	960.2
	Advantage4.1 (General)					Advantage4.1 (Prior)				
G1	-4	-1	-4.0	-4	0.1	-68	-53	-68.0	-68	0.2
G2	-9	-2	-7.1	-7	1.0	-495	-276	-431.0	-441	42.0
G3	-16	-2	-10.9	-11	1.7	-2064	-915	-1560.6	-1553	127.4
G4	-22	-2	-15.2	-15	2.6	-5776	-2779	-4428.6	-4525	347.4
G5	-29	3	-17.8	-18	4.0	-12568	-6093	-10258.4	-10407	845.6

We make the following observations from our empirical tests:

- The 2000Q and Advantage were able to produce the optimal solution up to G_3, where as the 2X was only able to produce the optimal solution up to G_2
- There is general improvement (a better lower bound) on the worst solution returned
- There is general improvement in the mean and median solutions returned with the newer annealers, with the exception of Advantage on G_4
- The Advantage was able to return valid, but non-optimal, solutions with our general formulation up to and including G_5

ICCS Camera Ready Version 2022
To cite this paper please use the final published version:
DOI: 10.1007/978-3-031-08760-8_13

While embeddings for G_6 and G_7 were identified on Advantage further analysis was not conducted given the decline in solution quality beyond the G_4 and G_5 graphs.

Table 2: Comparison of Valid Solutions returned by Quantum Annealers

(a) Valid Solutions Returned by 2000Q

Graph	Num. of Valid Sols.	
	Prior	General
G1	9959	9992
G2	4418	9561
G3	21	5575
G4	0	1516

(b) Valid Solutions Returned by Advantage1.1

Graph	Num. of Valid Sols.	
	Prior	General
G1	9987	10000
G2	2864	8509
G3	50	3511
G4	0	123
G5	0	2

(c) Valid Solutions Returned by Advantage4.1

Graph	Num. of Valid Sols.	
	Prior	General
G1	9998	9997
G2	3062	8821
G3	59	3255
G4	1	456
G5	0	7

The general formulation produced a greater number of valid solutions, as shown in Table 2. The newer Advantage architecture produced a reduced number of valid solutions compared to 2000Q. For example we obtained 1516 valid solutions on the 2000Q versus 123 on Advantage1.1 and 456 on Advantage4.1 using our general formulation for the G_4 graph. Even though Advantage returned fewer valid solutions, it still produced a better overall result, achieving a solution of -22 versus the -21 obtained on the 2000Q. The driver of this unexpected result is not clear, although Advantage4.1 closes this gap slightly. Potentially the more complex QPU architecture of Advantage compromises with an increased variability in results (noise), noting generally higher standard deviation values. A key benefit of Advantage is an increased connection density over the previous Chimera architecture, leading to easier identification of minor embeddings and both reduced total number and overall length of chains required.

Table 3 shows the number of returned samples, for each graph size, that contain at least one chain break, keeping in mind that chain breaks were resolved by majority voting. It was noted during testing that the number of samples that contained chain breaks, from a batch of 10,000, was rather variable. In particular, for G_3 the number of samples containing chain breaks would sometimes be higher for sample batches on the 2000Q and other times be higher for Advantage. This overlap in chain break occurrence is not entirely unexpected given that both the 2000Q and Advantage require a similar number of chains for the embedding, 60 and 50 respectively. However, at the scale of G_4 the benefits are clear, with Advantage typically suffering from only half as many chain breaks as the 2000Q.

Table 3: Number of Chain Breaks for Each Graph Size on different formulations and architectures. G_5 does not fit on $2000Q$.

Graph	# of Chain Breaks			
	2000Q		Advantage1.1	
	Prior	General	Prior	General
G1	13	4	0	0
G2	208	21	93	31
G3	440	594	739	431
G4	3648	3603	1583	1503
G5	-	-	5859	5862

ICCS Camera Ready Version 2022
To cite this paper please use the final published version:
DOI: 10.1007/978-3-031-08760-8_13

7 Energy Gaps

As noted in Section 1 QA generalises AQC and inhabits a regime that is intermediate between the idealised assumptions of universal AQC and unavoidable experimental compromises. As such we are unable to rely on the adiabatic theorem to ensure that an evolving quantum system will remain in its ground state. For non-adiabatic systems, as the energy gap between two states of a quantum system decreases, the likelihood that the system will 'jump', or more precisely undergo a diabatic transition, from one to state to another [28] increases. This possibility of diabatic transition is directly related to the likelihood that the system obtains the global solution.

Being able to determine if a problem suffers, or will suffer at larger scales, from a reducing gap between the first and second eigenvalues would be informative as to its suitability to QA. However, determining the minimum gap is not easy, in fact being able to calculate this gap would generally imply that the problem could be solved directly.

Given the limitations of calculating eigenstates, and corresponding eigenvalues, for the G_2 and beyond, we produce a number of interim graphs between the G_1 and G_2. These graphs attempt to replicate the inherent structure of this family of graphs, while providing a number of interim data points to assess the relationship between the minimum energy gap and number of variables.

7.1 Landau-Zener Formula

To investigate the scaling of the minimum energy gap we utilise the Landau-Zener (LZ) formula, which gives the probability of a diabatic transition between two energy states [28]. The LZ formula is intended for two-state quantum systems and employs several approximations. Even with these limitations the formula provides a useful tool to gain insight into how diabatic transitions may behave for varying graph sizes. The LZ formula along with supporting calculations are shown in Equations 6, 7 and 8 [25].

$$P_D = e^{-2\pi\Gamma} \tag{6}$$

$$\Gamma = \frac{a^2/\hbar}{\left|\frac{\partial}{\partial t}(E_2 - E_1)\right|} = \frac{a^2/\hbar}{\left|\frac{dq}{dt}\frac{\partial}{\partial q}(E_2 - E_1)\right|} = \frac{a^2}{\hbar|\alpha|} \tag{7}$$

$$\Delta E = E_2(t) - E_1(t) \equiv \alpha t \tag{8}$$

The quantity a is half the minimum energy gap, in our case the minimum energy gap between the first and second eigenstate. For the calculation of α in Equation 8 we assume a linear change in the gap between eigenvalues as defined in Equation 9.

$$\alpha = \frac{\text{Initial Gap - Minimum Gap}}{\text{Time to Minimum Gap}} \tag{9}$$

A decreasing minimum energy gap a drives the exponent in Equation 6 to zero and hence the probability of a diabatic transition, P_D, to 1.

ICCS Camera Ready Version 2022
To cite this paper please use the final published version:
DOI: 10.1007/978-3-031-08760-8_13

7.2 Modified Graph Family

The calculation of eigenvalues quickly becomes infeasible as the size of the system increases. Given that the graph family we have been utilising, G_n, scales in accordance with $(n+1)^3$ we subsequently require a matrix of size $2^{(n+1)^3} \times 2^{(n+1)^3}$ to represent the quantum system. As a result, even calculating eigenstates for the G_2 (27 variables) was beyond the capability of our consumer hardware. Given this limitation we constructed a number of 'interim' graphs, between G_1 and G_2, that increase in size while preserving key structural elements such as sparse outer layers and a denser connecting layer.

The graphs we utilise to investigate energy gaps are shown in Figure 2 and range in size from 8 to 22 variables (edges). For each of these graphs the optimal solution to the maximum matching problem is still to select all the edges in the sparse outer layers.

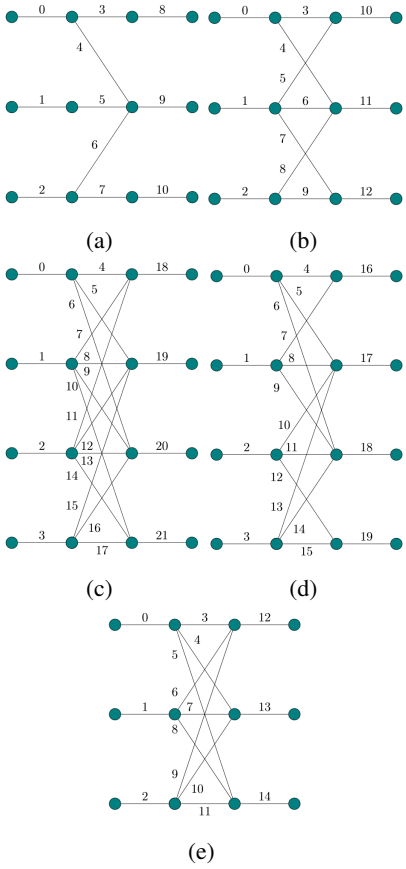

Fig. 2: (a), (b), (c), (d) and (e) show the interim graphs utilised to investigate the minimum energy gap

7.3 Eigenvalue Calculation

To determine the minimum energy gap between the ground state and first excited state we calculate the eigenvalues using the following process.

Construct Initial Hamiltonian: As per Equation 1 we form the initial Hamiltonian which is the sum of Pauli x matrices, $\hat{\sigma}_x$, see Equations 10 and 11.

$$H_i = \sum_i \hat{\sigma}_x^{(i)} \tag{10}$$

$$\hat{\sigma}_x^{(i)} \equiv \mathbb{I}_1 \otimes \cdots \otimes \mathbb{I}_{i-1} \otimes \hat{\sigma}_x^{(i)} \otimes \mathbb{I}_{i+1} \otimes \cdots \otimes \mathbb{I}_n \tag{11}$$

Obtain Biases and Couplers and Scale: To obtain the relevant biases and couplers for the particular graph we first form the corresponding Q matrix using the form shown in Equation 5, noting we again use a value of $P = 2$ for off-diagonal values. Using D-Wave's Ocean libraries the matrix is then converted into a binary quadratic model and subsequently an Ising model. The linear biases, h_i, and quadratic couplers, J_i, are then extracted from this Ising model.

Construct Final Hamiltonian: As per Equation 1 we form the final Hamiltonian which is the sum of Pauli z matrices, $\hat{\sigma}_z$, over both the biases, h_i, and couplers, $J_{i,j}$, see Equations 12 and 13.

ICCS Camera Ready Version 2022
To cite this paper please use the final published version:
DOI: 10.1007/978-3-031-08760-8_13

$$H_f = \sum_i h_i \hat{\sigma}_z^{(i)} + \sum_{i>j} J_{i,j} \hat{\sigma}_z^{(i)} \hat{\sigma}_z^{(j)} \tag{12}$$

$$\hat{\sigma}_z^{(i)} \hat{\sigma}_z^{(j)} \equiv \mathbb{I}_1 \otimes \cdots \otimes \mathbb{I}_{i-1} \otimes \hat{\sigma}_z^{(i)} \otimes \mathbb{I}_{i+1} \otimes \cdots \otimes \mathbb{I}_{j-1} \otimes \hat{\sigma}_z^{(j)} \otimes \mathbb{I}_{j+1} \otimes \cdots \otimes \mathbb{I}_n \tag{13}$$

Define the System Evolution: The evolution of the system occurs as per Equation 14, where t_f is the annealing duration, nominally being $20\mu s$ and $t \in [0, t_f]$. The value of s is then used to determine the corresponding $A(s)$ and $B(s)$ (units of GHz) as per the annealing schedule [7].

$$H(s) = A(s)H_i + B(s)H_f \tag{14}$$

Calculate Eigenvalues: The first (ground state) and second (first excited state) eigenvalues of H, from Equation 14, are calculated as a function of s. With these eigenvalues the initial gap, when $s = 0$, can be calculated and also the value of s that corresponds to the smallest gap. With these values the value of α can be calculated using Equation 9 and the fact that the time to the minimum energy gap can be calculated by $t = st_f$.

7.4 Energy Gap Results and Expected Diabatic Transition Probability

In Figure 3 we plot the minimum energy gap between the first and second eigenvalue with a fitted exponential trendline. While the range of graph sizes utilised is narrow, the data suggest that it is plausible that the minimum energy gap decreases exponentially with graph size. If these results are indicative of the scaling of the minimum energy gap for larger G_n graphs we would expect that the probability of diabatic transitions during annealing would increase dramatically.

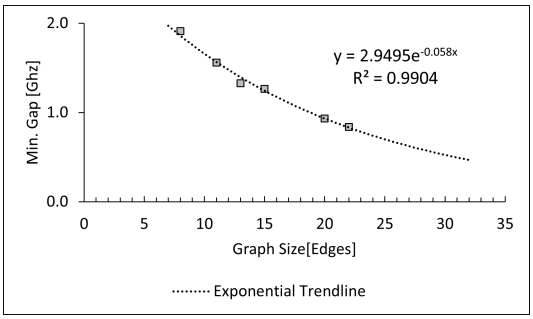

Fig. 3: Minimum Energy Gaps for Varying Graph Sizes (with Exponential Trendline)

The other factor that impacts the diabatic transition probability is the time until the minimum energy gap, with this value showing up in the denominator of Equation 9. This time varies slowly as a function of graph size on our interim graphs, but it is insufficient to offset an exponentially decreasing minimum energy gap. We also assume a constant initial energy gap of $19.6\ GHz$, which is based on the average initial energy gap for the interim graphs, with the initial gap ranging from $19.5\ GHz$ to $19.7\ GHz$.

ICCS Camera Ready Version 2022
To cite this paper please use the final published version:
DOI: 10.1007/978-3-031-08760-8_13

We now extrapolate the quantities obtained from the eigenvalues of the Hamiltonian for larger graphs. Using the LZ formula on the extrapolated quantities we calculate the expected diabatic transition probability for an annealing cycle. This procedure spares us from the need of simulating the quantum annealing process by integrating the Schrödinger equation.

The increase in diabatic transition probability corresponds to a decreasing likelihood that an annealing cycle won't be affected by a diabatic transition. Figure 4 plots the expected number of annealing cycles, out of 10,000 cycles (the default value), where a diabatic transition does not occur, based on our energy gap modelling (grey squares), versus the number of optimal solutions we actually obtained from our empirical tests on Advantage1.1 (black squares). We specifically compare to the results obtained from Advantage using our general formulation and an annealing duration of $20\mu s$.

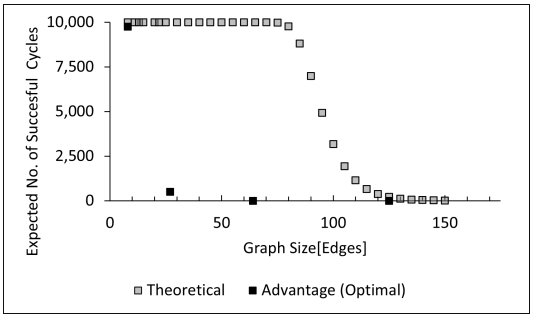

Fig. 4: Theoretical Expected No. of Successful Annealing Cycles (out of 10,000) versus Number of Optimal Solutions Returned from Advantage1.1

The results of the Advantage architecture are compatible with the theoretical result, once noise is taken into account. Between G_1 (8 edges) and G_2 (27 edges) there is a significant drop in the number of optimal solutions obtained and by G_3 only a single optimal solution is returned out of 10,000 annealing cycles and none for G_4. Our theoretical model indicates that obtaining optimal solutions, even for future hardware, is highly unlikely for G_5 (216 edges) and beyond.

7.5 Energy Gap Analysis Limitations

We acknowledge that in our probing of the behaviour of the minimum energy gap we have made a number of assumptions, namely that our fabricated graphs are representative of the original graph family, that the minimum energy gap and time to minimum energy gap follow an exponential and logarithmic relationship respectively and that the results we obtain can be extrapolated. Further to this, the LZ formula is based on a two-state quantum system with additional assumptions that ignore external impacts. Our systems are clearly multi-state, with degenerate energy levels occurring from the first excited state, and as such diabatic transitions may occur between any states of the system. As such, our analysis is not intended to be a precise calculation of theoretical behaviour, but it is meant to capture the possible scaling of the problem, to provide initial insights into how the diabatic transition probability scales for large graphs and to give an indication of the quantum complexity of our problem, and thus the suitability of such a problem as a benchmark for QA hardware.

There are likely a number of additional factors, as discussed in [11], that further contribute to imperfect annealing, such as thermal excitation, unintended qubit cou-

ICCS Camera Ready Version 2022
To cite this paper please use the final published version:
DOI: 10.1007/978-3-031-08760-8_13

plings, errors in couplings and biases within the implemented Hamiltonian and decoherence in energy eigenstates. It is not unexpected that our empirical results fall short of our theoretical model. However, we do believe that even given the limitations and assumptions of our approach that our analysis lends credence to the possibility that larger instances of our target problem may become intractable for future generations of QA hardware. At the very least, the minimum energy gap of benchmarking problems should be considered when assessing performance of quantum annealers to ensure performance improvements can be adequately discerned.

8 Discussion of Future Work

The empirical tests we have conducted on the latest QA hardware from D-Wave are an extension of prior work from [23]. It is likely that performance could be improved by further considering other annealing variables. For instance, custom annealing schedules, chain strengths, chain break resolution methods and annealing offsets [27] (adjustment of annealing path per qubit) could be optimised for improved results. We leave these optimisations for future work where the impacts of such optimisations can be contrasted to our implementation to assess the benefits of parameter tuning.

Secondly, our investigation into energy gap scaling utilised fabricated graphs up to a size of 22 variables (edges). It would be insightful to extend the analysis up to the G_2 graph, as it would provide a direct point of comparison to the original graph family and assist with validating the scaling behaviour of the maximum matching problem on the G_n graph family.

9 Conclusion

We have extended the prior work of [23] and the optimisation problem of maximum cardinality matching to the latest QA hardware from D-Wave, the 2000Q and Advantage quantum annealers. In doing so we propose an improved version of the QUBO formulation of this problem, specifically we modify the ratio of diagonal to off-diagonal terms of the Q matrix so that the formulation is applicable to arbitrary graph structures. We find that this formulation produces significantly more valid solutions. With the increased number of qubits and improved topology we also obtain empirical results for larger problem instances, although solution quality at these scales remains notably poor. We do note that the minor embeddings produced for these problems are far more compact on the newer Pegasus topology.

Our testing shows improvements in the capability of QA hardware to solve combinatorially difficult optimisation problems. Our results demonstrate a general improvement in the lower bound of solution quality and importantly we observe that the 2000Q and Advantage are capable of producing the optimal solution for G_3, whereas [23] were unable to do so using the 2X quantum annealer.

Following from our empirical tests we probe the behaviour of the minimum energy gap of our target problem by formulating a number of 'interim' graphs, that maintain key structural elements. We numerically calculate the first and second eigenvalues over an evolutionary path that replicates the behaviour of the Advantage1.1 quantum

ICCS Camera Ready Version 2022
To cite this paper please use the final published version:
DOI: 10.1007/978-3-031-08760-8_13

annealer. These eigenvalues are then used to calculate the minimum energy gaps that occur during annealing. To further investigate the minimum energy gap behaviour for larger graphs we assume that the minimum energy gap decreases exponentially, which our data support. We combine this with the LZ formula to calculate the probability of a diabatic transition during an annealing cycle. We observe that even with this theoretical approach, the increasing likelihood of diabatic transitions as graph sizes increase suggests that optimal solutions for this problem on graph sizes of G_5 and above are unlikely to be achieved in the near term.

Ultimately our empirical results show improvement in the capability of QA hardware with the 2000Q and Advantage being able to solve the maximum cardinality matching problem for a G_3, which escaped previous generations. However, our further investigations into energy gaps and diabatic transitions raises questions about the suitability of maximum cardinality matching problem on this graph family as a benchmarking tool for QA hardware, as it potentially lacks the nuance required to identify meaningful performance improvements between generations of QA hardware. We hope that the methods developed in our work can be used to guide the design of better benchmarking problems for QA hardware.

Acknowledgments. We would like to thank Professor Tat-Jun Chin for his support, expertise and feedback that was invaluable in producing this work.

References

1. Albash, T., Lidar, D.A.: Adiabatic quantum computation. Reviews of Modern Physics **90**(1) (Jan 2018). https://doi.org/10.1103/revmodphys.90.015002, http://dx.doi.org/10.1103/RevModPhys.90.015002
2. Benioff, P.: The computer as a physical system: A microscopic quantum mechanical hamiltonian model of computers as represented by turing machines. Journal of statistical physics **22**(5), 563–591 (1980)
3. Benioff, P.: Quantum mechanical hamiltonian models of turing machines. Journal of statistical physics **29**(3), 515–546 (1982)
4. Benioff, P.: Quantum mechanical models of turing machines that dissipate no energy. Physical review letters **48**(23), 1581–1585 (1982)
5. Cai, J., Macready, W.G., Roy, A.: A practical heuristic for finding graph minors (2014)
6. D-Wave Systems Inc.: Programming the D-Wave QPU: Parameters for Beginners. 14-1045A-A
7. D-Wave Systems Inc.: QPU-Specific Anneal Schedules – D-Wave Systems. https://docs.dwavesys.com/docs/latest/doc_physical_properties.html, [Accessed: 5 Feb 2022]
8. Dyakonov, M.: When will useful quantum computers be constructed? not in the foreseeable future, this physicist argues. here's why: The case against: Quantum computing. IEEE spectrum **56**(3), 24–29 (2019)
9. Farhi, E., Goldstone, J., Gutmann, S., Sipser, M.: Quantum computation by adiabatic evolution (2000)
10. Feynman, R.P.: Simulating physics with computers. International journal of theoretical physics **21**(6-7), 467–488 (1982)
11. Gardas, B., Dziarmaga, J., Zurek, W.H., Zwolak, M.: Defects in quantum computers. Scientific reports **8**(1), 4539–10 (2018)

ICCS Camera Ready Version 2022
To cite this paper please use the final published version:
DOI: 10.1007/978-3-031-08760-8_13

12. Glover, F., Kochenberger, G., Du, Y.: Quantum bridge analytics i: a tutorial on formulating and using qubo models. 4OR **17**(4), 335–371 (2019)
13. King, A.D., Raymond, J., Lanting, T., Isakov, S.V., Mohseni, M., Poulin-Lamarre, G., Ejtemaee, S., Bernoudy, W., Ozfidan, I., Smirnov, A.Y., Reis, M., Altomare, F., Babcock, M., Baron, C., Berkley, A.J., Boothby, K., Bunyk, P.I., Christiani, H., Enderud, C., Evert, B., Harris, R., Hoskinson, E., Huang, S., Jooya, K., Khodabandelou, A., Ladizinsky, N., Li, R., Lott, P.A., MacDonald, A.J.R., Marsden, D., Marsden, G., Medina, T., Molavi, R., Neufeld, R., Norouzpour, M., Oh, T., Pavlov, I., Perminov, I., Prescott, T., Rich, C., Sato, Y., Sheldan, B., Sterling, G., Swenson, L.J., Tsai, N., Volkmann, M.H., Whittaker, J.D., Wilkinson, W., Yao, J., Neven, H., Hilton, J.P., Ladizinsky, E., Johnson, M.W., Amin, M.H.: Scaling advantage over path-integral monte carlo in quantum simulation of geometrically frustrated magnets. Nature communications **12**(1), 1113–1113 (2021)
14. Kitaev, A.: Fault-tolerant quantum computation by anyons. Annals of physics **303**(1), 2–30 (2003)
15. Korte, B.: Combinatorial Optimization Theory and Algorithms. Algorithms and Combinatorics, 21, Springer Berlin Heidelberg, Berlin, Heidelberg, 5th ed. 2012. edn. (2012)
16. Lucas, A.: Ising formulations of many np problems. Frontiers in physics **2** (2014)
17. Morita, S., Nishimori, H.: Mathematical foundation of quantum annealing. Journal of mathematical physics **49**(12), 125210–125210–47 (2008)
18. Nielsen, M.A., Chuang, I.L.: Programmable quantum gate arrays. Physical review letters **79**(2), 321–324 (1997)
19. Nimbe, P., Weyori, B.A., Adekoya, A.F.: Models in quantum computing: a systematic review. Quantum information processing **20**(2) (2021)
20. Raussendorf, R., Briegel, H.J.: A one-way quantum computer. Physical review letters **86**(22), 5188–5191 (2001)
21. SANTORO, G.E., MARTONAK, R., TOSATTI, E., CAR, R.: Theory of quantum annealing of an ising spin glass. Science (American Association for the Advancement of Science) **295**(5564), 2427–2430 (2002)
22. Sasaki, G., Hajek, B.: The time complexity of maximum matching by simulated annealing. Journal of the ACM **35**(2), 387–403 (1988)
23. Vert, D., Sirdey, R., Louise, S.: Revisiting old combinatorial beasts in the quantum age: Quantum annealing versus maximal matching. vol. 12142 LNCS (2020). https://doi.org/10.1007/978-3-030-50433-5_37, main
24. Vinci, W., Lidar, D.A.: Non-stoquastic hamiltonians in quantum annealing via geometric phases. npj quantum information **3**(1), 1–6 (2017)
25. Wittig, C.: The landau-zener formula. The journal of physical chemistry. B **109**(17), 8428–8430 (2005)
26. Yarkoni, S., Neukart, F., Tagle, E.M.G., Magiera, N., Mehta, B., Hire, K., Narkhede, S., Hofmann, M.: Quantum shuttle: Traffic navigation with quantum computing (2020)
27. Yarkoni, S., Wang, H., Plaat, A., Bäck, T.: Boosting quantum annealing performance using evolution strategies for annealing offsets tuning. In: Quantum Technology and Optimization Problems. pp. 157–168. Lecture Notes in Computer Science, Springer International Publishing, Cham (2019)
28. Zener, C.: Non-adiabatic crossing of energy levels. Proceedings of the Royal Society of London. Series A, Containing papers of a mathematical and physical character **137**(833), 696–702 (1932)

ICCS Camera Ready Version 2022
To cite this paper please use the final published version:
DOI: 10.1007/978-3-031-08760-8_13